Characterization of the Morning Transition over the Gentle Slope of a Semi-Isolated Massif

SOFIA FARINA,[a,b] MATTIA MARCHIO,[a,b] FRANCESCO BARBANO,[c] SILVANA DI SABATINO,[c] AND DINO ZARDI[a,b]

[a] Atmospheric Physics Group, Department of Civil, Environmental and Mechanical Engineering, University of Trento, Trento, Italy
[b] Center Agriculture Food Environment (C3A), University of Trento, Trento, Italy
[c] Department of Physics and Astronomy, Alma Mater Studiorum, University of Bologna, Bologna, Italy

ABSTRACT: This paper investigates the surface-layer processes associated with the morning transition from nighttime downslope winds to daytime upslope winds over a semi-isolated massif. It provides an insight into the characteristics of the transition and its connection with the processes controlling the erosion of the temperature inversion at the foot of the slope. First, a criterion for the identification of days prone to the development of purely thermally driven slope winds is proposed and adopted to select five representative case studies. Then, the mechanisms leading to different patterns of erosion of the nocturnal temperature inversion at the foot of the slope are analyzed. Three main patterns of erosion are identified: the first is connected to the growth of the convective boundary layer at the surface, the second is connected to the descent of the inversion top, and the third is a combination of the previous two. The first pattern is linked to the initiation of the morning transition through surface heating, and the second pattern is connected to the top-down dilution mechanism and so to mixing with the above air. The discriminating factor in the determination of the erosion pattern is identified in the partitioning of turbulent sensible heat flux at the surface.

SIGNIFICANCE STATEMENT: The purpose of this study is to improve our understanding of the thermally driven slope circulations with a focus on the unsteady processes associated with the morning transition and the erosion patterns of the nocturnal temperature inversion, so far in the literature less investigated and understood than the evening transition. Understanding this diurnal process will advance our abilities to model it and to improve the accuracy of weather forecasting in complex terrain.

KEYWORDS: Turbulence; Energy budget/balance; Mountain meteorology

1. Introduction

Over mountainous terrain, under unperturbed synoptic-scale weather (i.e., anticyclonic conditions), the atmospheric boundary layer responds to the diurnal cycle of radiative forcing developing daily periodic wind systems at different spatial scales (Whiteman 2000; Giovannini et al. 2017; Lehner and Rotach 2018). These wind systems evolve during the day, variously interacting among them. However, all of them undergo a typical wind reversal twice per day, from the diurnal upslope/upvalley directions to the nocturnal downslope/downvalley directions, and vice versa (Atkinson 1981; Whiteman 2000; Zardi and Whiteman 2013). In particular, the diurnal development of slope winds is closely tied to the thermal structure of the

boundary layer within the adjacent valleys and plains and connected to the daily cycles of buildup and breakdown of surface temperature inversions (Ayer 1961; Banta 1984, 1986; Freytag 1987; Vergeiner and Dreiseitl 1987; Kossmann et al. 1998; Whiteman 2000; Rampanelli et al. 2004). For these reasons, slope and valley winds are often referred to as thermally driven flows.

Thermally driven flows have been extensively studied in the past, starting from the analysis of data from field observations, with the aid of analytical models (Kuwagata and Kondo 1989; Chow et al. 2013; Reuten et al. 2005; Lehner and Rotach 2018; Serafin et al. 2020). More recent studies have extensively taken advantage from progress in numerical modeling (Kuwagata and Kimura 1997; Serafin and Zardi 2010; Wagner et al. 2015; Cintolesi et al. 2021).

A variety of thermally driven flows may be observed in the mountains, originating from a broad diversity of complex terrains. Indeed, each wind system is strongly marked by the distinctive characteristics of the terrain where it develops. However, all of them originate from surface heat fluxes

---

occurring on the nonhorizontal terrain underneath, where heat and momentum budgets at every point are strongly characterized by the local slope. In other words, all these flows include, at local scale, surface features amenable to slope winds. Hence, processes developing over simple slopes provide basic prototypes, at the local scale, for the driving processes of all the other winds. This makes the investigation of their physical mechanisms crucial for a basic understanding of other thermally driven wind systems.

Both upslope (or anabatic) and downslope (or katabatic) winds are driven by the daily cycle of surface sensible heat flux (SH). This is typically stronger during daytime than at night. Hence anabatic winds usually display peak velocities higher than their nocturnal counterparts and are associated with deeper boundary layers (Whiteman 2000). On the other hand, katabatic winds occur within particularly shallow layers, and reach maximum speeds around 1–3 m above ground (Doran and Horst 1981, 1983; Horst and Doran 1986, 1988; Mahrt and Larsen 1990; Whiteman 2000; Charrondière et al. 2020, 2022). Two natural transitional phases between katabatic and anabatic regimes occur, one in the morning and the other in the evening, following sunrise and sunset, respectively. The available literature on the evening transition offers quite a comprehensive overview on the driving mechanisms and associated phenomena, as well as on their sensitivity to different environmental conditions (e.g., Whiteman 2000; Brazel et al. 2005; Nadeau et al. 2013). On the contrary, the morning transition and the daytime evolution of the anabatic wind have been less investigated and understood (Hunt et al. 2003; Rampanelli et al. 2004). Various reasons make upslope winds more challenging to capture: in particular, the diurnal circulation is more rarely stationary, as it easily undergoes faster adjustments to the stronger and more variable surface heat fluxes, typically observed during daytime than during nighttime. Also, it is more difficult to isolate them from the overlying circulations induced by widespread convection. Nevertheless, understanding the diurnal slope winds is fundamental for several applications in complex terrain, such as air quality management (Giovannini et al. 2020; Zardi et al. 2021), as well as for numerical weather predictions, especially in connection with convection initiation (Whiteman and Allwine 1985; Rendón et al. 2015; De Wekker and Kossmann 2015; De Wekker et al. 2018; Serafin et al. 2018).

Despite various investigations on the subject, there are still open questions concerning the morning initiation of slope winds. In particular, there is no conclusive evidence about which key mechanism triggers the onset of the upslope flows and where the flow first starts along the slope. Banta (1984) was among the first to observe the onset of an upslope flow both at midheight and at the foot of a slope in South Park, a broad and flat basin in the Colorado Rocky Mountains, during the South Park Area Cumulus Experiment (SPACE-77). On the contrary, Brehm and Freytag (1982) during the "Slopewind Experiment Innsbruck October 1978" observed that in a narrow alpine slope the onset was always occurring in the upper part of the slope. Later studies by Papadopoulos and Helmis (1999) identified the initiation at midslope on the steep eastern slope of Mount Hymettos (Greece). They outlined two

possible competing mechanisms controlling the breakup of the surface inversion at the foot of a steep slope: (i) the warming of the air from above through mixing with (or replacement by) the overlying air (top/down dilution), and (ii) the warming of the surface air from below due to surface heating. These two different mechanisms usually lead to distinct transition patterns exhibiting different characteristics. The warming from above, where air entrainment at the top of the katabatic layer generates mixing, leads to top-down destruction of the katabatic flow and to the replacement with the upslope flow (Atkinson 1981; Papadopoulos and Helmis 1999). In the other mechanism, that is, the warming from below, the katabatic flow dissipates with the inversion layer as the surface becomes warmer than the overlying air, driving a newly formed upslope flow. The initiation of the upslope flow follows the erosion, sliding in opposition to the dissipating katabatic flow. As the erosion proceeds, the upslope flow layer grows, eroding the inversion layer and driving a horizontal divergence of the katabatic flow generating a cold advection (Papadopoulos and Helmis 1999).

The winds in the inversion layer usually exhibit moderate intensities. However, above the top of the inversion layer, the winds can be strong, leading to strong shear and turbulent mixing there. This mixing is a key factor for eroding the inversion layer from above. This process usually persists through the next morning and contributes to the inversion destruction after sunrise. This process is faster than the warming from the ground, and the inversion-layer lapse rate remains constant. The upslope motions first develop in the higher layers. Then, as the mixing proceeds toward the surface, the anabatic flow slides above the katabatic, compressing the inversion layer and driving a horizontal cold advection (Papadopoulos and Helmis 1999). The other mechanism is the warming from below: here the katabatic motion starts ceasing when the surface becomes warmer than the overlying air, and the newly developing upslope motion causes a horizontal cold advection to compensate for the surface heating.

However, a key question still remains open: which ambient conditions are conducive to either mechanism? To answer this question, one further aspect needs to be taken into account, that is, the connection with the breakup of the nocturnal temperature inversion in the region adjacent to the slope, such as a valley or a plain. Concerning this issue, an illuminating contribution to our understanding of erosion patterns was provided by Whiteman (1982) from observations of the nocturnal inversion breakup in a deep valley in Colorado. Three main patterns were identified: (i) the upward growth of a convective boundary layer from the ground, (ii) the descent of the inversion top, and (iii) a combination of the previous ones. The pattern (i) is characterized by the heating of the ground surface resulting in a heat flux reversal; here, the convective boundary layer starts growing at the expense of the preexisting stable layer. The opposite process is found in pattern (ii), in which warm air penetrates the inversion layer from above. These patterns were reproduced by Whiteman and McKee (1982) with a simple thermodynamic model for the inversion breakup in a deep valley, accounting for energy partitioning criteria and valley geometry.

Further experiments, performed in deep valleys, identified the main mechanism for inversion erosion in the warming associated with subsidence compensating for the removal of air

at lower levels by upslope winds (Kuwagata and Kimura 1995, 1997; Whiteman et al. 2004; Brehm and Freytag 1982). On the other hand, similar analyses performed on broad valleys revealed that the most frequent scenario consists in a combination of the upward growth of the convective boundary layer and the descent of the inversion top (Triantafyllou et al. 1995; Banta and Cotton 1981). Numerical studies on the erosion of the nocturnal inversion (Bader and McKee 1983, 1985; Colette et al. 2003; Leukauf et al. 2015; Ye et al. 1987) tested several different valley configurations and concluded that the descent of the inversion top is more pronounced in deeper valleys. Zoumakis and Efstathiou (2006a,b) proposed a refinement of the thermodynamical model by Whiteman and McKee (1982), introducing new analytical relations describing the evolution of the boundary layer height, and evaluating the time required to erode the inversion through semiempirical parameterizations of radiation and surface energy budgets.

Nevertheless, studies linking the transition mechanisms to the erosion of the inversion are still limited, mostly due to the scarcity of data available from targeted field experiments. Many field campaigns investigating slope winds deployed most of the instrumentation along the slope. As a result, information about the vertical structure of the ambient atmosphere in the adjacent areas has often been neglected.

The present work investigates the connection between the erosion of the inversion and the development of the anabatic flow over a slope, testing the driving mechanisms proposed by Papadopoulos and Helmis (1999). In particular, we focused on the following scientific questions:

- Which are the main characteristics of the morning transition on a gentle slope?
- Which are the main mechanisms of erosion of the nocturnal inversion at the foot of the slope?
- Which are the connections between the mechanisms of inversion breakup at the foot of the slope and those driving the morning transition on the slope?

To address these questions the present study adopted as target area the east-facing gentle slope of a semi-isolated massif facing an open valley, where an unprecedented extensive dataset was available from the Mountain Terrain Atmospheric Modeling and Observations (MATERHORN) Program experiment (Fernando et al. 2015). The project enabled monitoring a variety of processes occurring both along the slope of the massif (a topographic configuration never deeply investigated before) and in the adjacent valley. Such a layout offered an ideal spot for investigating the driving mechanisms controlling the transition, avoiding major interferences from other topographic factors in the surroundings, as opposed to deep valleys, where the effects of one sidewall onto the other (e.g., shielding, shading) interfere in localizing the initiation of the transition. This interference makes it extremely difficult to detect and isolate the role of the vertical structure of the ambient atmosphere.

The article is organized as follows: Section 2 outlines the dataset and the methods used in the data analysis. In section 3, the results from the investigation of the inversion erosion and the morning transition are presented. Section 4 carries out the

discussion of results and outlines the connections between them. Section 5 presents the conclusions and highlights open questions and possible future developments.

2. Data and methods

a. The MATERHORN dataset

The MATERHORN Program was a cooperative effort promoted by five research institutions (Fernando et al. 2015). The program was designed to investigate a variety of processes characterizing mountainous terrain, in view of improving our modeling capabilities for weather predictions in complex terrain. As part of the program, the experimental activity, MATERHORN-X, included two major campaigns, respectively, in autumn (September–October 2012) and in spring (May 2013). The autumn campaign was characterized by a majority of quiescent, dry, calm weather periods, dominated by clear diurnal cycles of daytime heating and nighttime cooling. On the contrary, the spring campaign displayed highly variable and often perturbed synoptic conditions (Fernando et al. 2015). The target site for both campaigns was the Granite Mountain Atmospheric Science Testbed (GMAST) of the U.S. Army Facility of Dugway Proving Ground (DPG), located within the Dugway Valley, a wide, open, and gentle-sloping valley declining into a vast plain, approximately 140 km southwest of Salt Lake City, Utah (Fig. 1a).

The focus of the present investigation is around the Granite Mountain, an almost isolated massif separated from the southern topographic chain by a gap and declining in all other directions into an extremely wide valley (Fig. 1a). Granite Mountain has a length of 11.8 km in the north–south direction, a base width of 6.1 km at the largest cross section, and a peak elevation of 840 m above the valley floor level (1300 m MSL). Specifically, the analyzed area of the present study is the east-facing slope of Granite Mountain, a gentle incline displaying local slope angles ranging between 3° and 6° (Table 1).

The instrumentation was installed along the incline, as outlined schematically in Figs. 1b and 2, and consisted of five towers, designated as ES1–ES5 from lower to higher elevation. These towers were placed at approximately 600–700 m from each other, along the steepest descent line, with the only exception of the ES1, which was located on the valley floor, along the same line. All the towers ES1–ES5 were equipped with fast-response three-axial sonic anemometers (Young 81000, for ES2 and ES4, and Campbell Scientific CSAT3 for all of the others) sampling at 20 Hz, and slow-response temperature and relative humidity probes (KH20 thermohygrometers) sampling at 1 Hz. Each tower was equipped with at least five measurement levels (see Table 1 for details). Radiation and energy fluxes were collected at the ES3 and ES5 towers only, located at midslope, using a Net Radiometer CNR1-L and a Soil Heat Flux Plate HFP01SC-L, respectively.

To integrate the flux-tower measurements with observations representative of the ambient conditions, data were also collected using a tethersonde (Vaisala TTS111) and a radiosonde (Graw DFM-09) at Sagebrush, 13 km northeast of the east slope (Fig. 1a). Vertical temperature profiles were measured by tethered balloon soundings up to a height of 400 m,
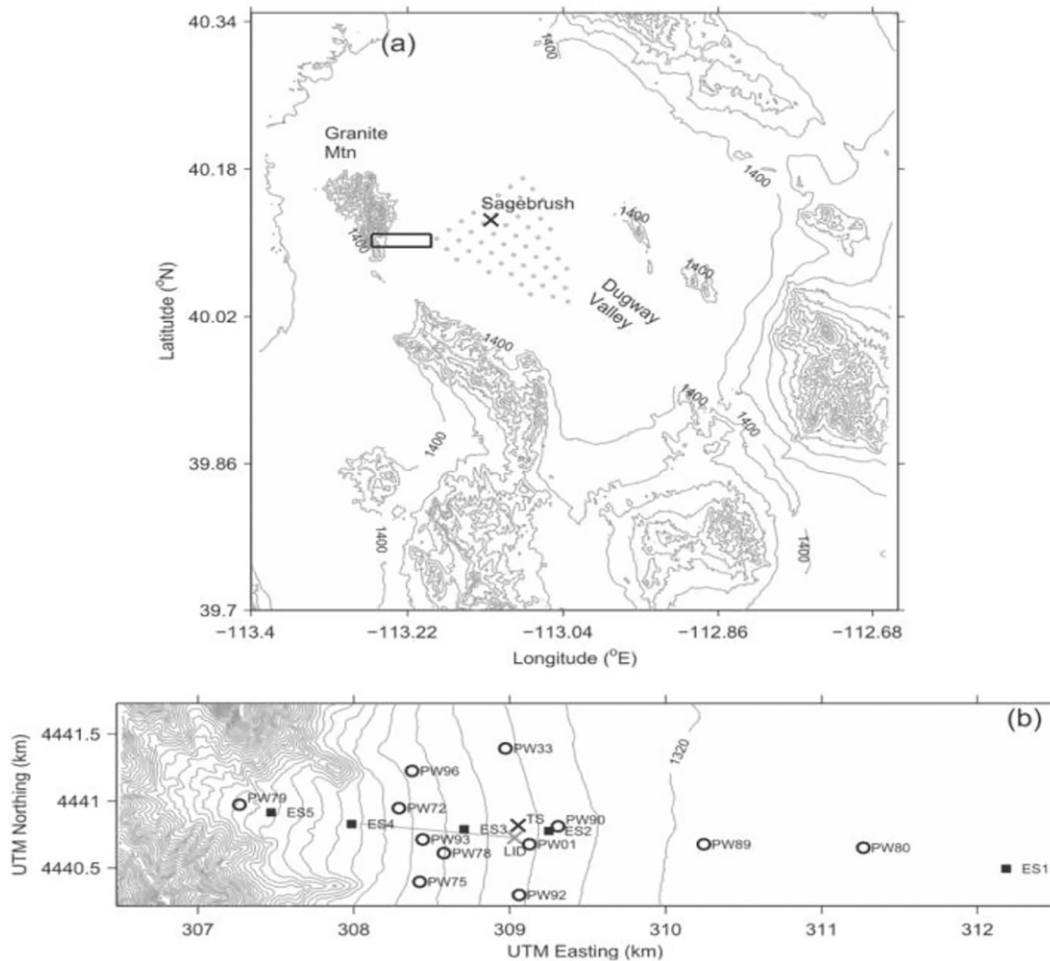
FIG. 1. (a) Map of the experimental sites of Granite Mountain and Dugway Valley, and (b) detailed map of the instrumented east sidewall (ES) of Granite Mountain and the locations of measurement sites. The symbols in (a) and (b) named Sagebrush and TS mark the locations of tethersonde measurements, LID refers to a lidar, and the gray dots in (a) show the network of mini-surface atmospheric measurement systems (miniSAMS) sites. In (b), the filled squares labeled ES show the locations of the five towers, and the open circles labeled PW show the locations of portable weather instrumentation data systems (PWIDS) surface stations. The isolines are drawn every 100 m in (a) and every 10 m in (b). the images in (a) and (b) and their captions are adapted from Lehner et al. (2015).

with several ascents (up to 15 per day) during the intensive observation periods (IOPs). Vertical profiles of temperature, pressure, wind speed, and wind direction were measured by a radiosonde, with at least eight full ascents per IOP.

b. Data processing

For the present analysis, datasets were preliminary checked to remove data containing unreliable values, or clearly affected by instrumental errors, based on threshold derived from typical ranges for the area. The velocity components measured with the sonic anemometers were also rotated, following the double rotation method developed by McMillen (1988), to align the reference frame to the streamlines. This double rotation was individually applied to each flux tower using the local azimuthal angles as specified in Table 1. As a result, in the local rotated

system the horizontal velocity components u, v, and w identify the along slope (approximately west–east), cross slope (approximately south–north) and slope normal wind velocity components, respectively.

To guarantee the overall robustness of the analysis without losing information on small-scale processes, all quantities were 5-min averaged unless otherwise specified. The high-frequency data collected by anemometers at 20 Hz were further averaged every 30 min. The double-averaging technique is commonly used in eddy covariance analysis to filter low-frequency components. It was successfully adopted in previous works on the same dataset of the present research (Barbano et al. 2022). Finally, second-order moments were computed using the eddy-correlation method on nondetrended values every 5-min time windows.

TABLE 1. Topographic characteristics of the sites where the towers were located along the east slope of Granite Mountain. The elevation, azimuth, and slope angle of the measurement sites are indicated along with the measurement levels on the towers. When two different series of measurement levels are indicated, they refer to the two seasons of measurements (fall 2012 and spring 2013, respectively).

Site	Elev	Azimuth	Slope angle	Levels
ES1	1313 m	83°	0.0°	1.95, 4.00, 8.10, 14.30, and 26.25 m
ES2	1338 m	95°	1.6°	0.50, 2.00, 5.00, 10.00, 16.00, 20.00, 25.00, and 32.00 m; 0.50, 3.00, 5.00, 7.00, 10.00, 16.00, 20.00, 23.00, 25.00, and 28.00 m
ES3	1354 m	75°	1.7°	0.50, 2.00, 5.00, 10.00, and 20.00 m; 1.00, 3.00, 4.00, 5.00, 6.00, 7.00, 8.00, 9.00, 10.00, 16.00, and 20.00 m
ES4	1394 m	104°	5.8°	0.61, 2.74, 5.79, 10.97, 20.73, 26.69 m
ES5	1433 m	120°	3.6°	0.55, 2.14, 5.13, 10.13, and 20.08 m; 0.55, 2.14, 5.13, 10.13, and 20.08 m

Using the computed turbulent fluxes, to identify the key characteristics of the morning transition and the proper conditions for the onset and development of an upslope flow, we investigated the energetics of the flow evaluating the surface energy balance (SEB) as

$$\dot{Q} = R_n - G - H - LE,$$

where $\dot{Q}$ is the total heat storage in the surface layer, R_n is the net all-wave surface irradiance, G is the ground heat flux, H is the sensible heat flux, and LE is the latent heat flux.

A specific postprocessing treatment was applied to the tethered-balloon data. An offset was evaluated to correct the elevation in the tethered-balloon ascents, whenever elevation values were recorded below local ground level, because of instrumental errors at the balloon takeoff. Vertical profiles collected by tethersonde were not averaged (except for data collected at the same altitude), to ensure regularly spaced values (i.e., one datum per meter).

3. Results

a. Slope wind days' selection and criteria

In view of observing peculiar features of daily periodic mountain winds, it is of utmost importance to isolate situations when weather conditions allow for strong surface heat fluxes, and large scale winds minimally perturb the development of pure thermally driven flows. Various criteria are available in the literature for the identification of days exhibiting weather conditions conducive to the full development of valley winds (Giovannini et al. 2017; Lehner et al. 2019) or, more generally, for the development of thermally driven circulations (Román-Cascón et al. 2019). However, no criteria have been specifically designed for slope winds. In particular, the method outlined by Giovannini et al. (2017) is based on the analysis of pressure, net radiation, wind direction, and intensity, as per the conditions reported in Table 2. Instead, Román-Cascón et al. (2019) suggested a more general method to identify situations favorable for a variety of thermally driven flows (including both valley winds and slope winds). This method considers, besides wind data, also synoptic wind speed and the rate of change of potential temperature at 700-hPa level, as well as daily rainfall accumulation (criteria are summarized in Table 2). Both methods include in the criteria for selecting
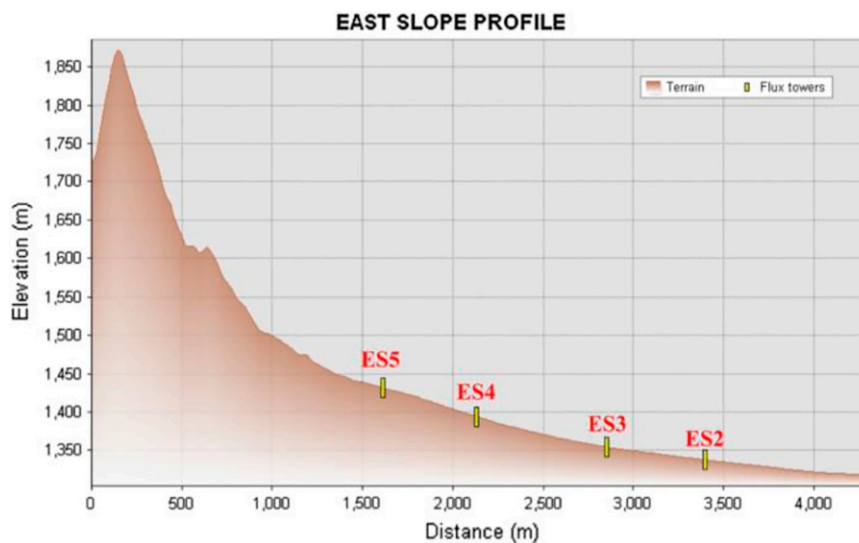

FIG. 2. Layout of the four towers along the ES of Granite Mountain (adapted from Grachev et al. 2016).

TABLE 2. Summary of the proposed criteria for the identification of slope wind days starting from an extended database; the methods proposed by Giovannini et al. (2017) and Romàn-Cascón et al. (2019) are reported for comparison.

Variable	Giovannini et al. (2017)	Román-Cascón et al. (2019)	Proposed method
Radiation	Global daily radiation > 50% of the max radiation of the month		Avg daily radiation > avg monthly radiation; avg daily shortwave radiation > avg monthly shortwave radiation
Pressure	Diurnal pressure range between 2.0 and 8.0 hPa		Avg daily pressure > avg monthly pressure
Synoptic conditions		Synoptic speed at 700 hPa < 9 m s^{-1} and equivalent potential temperature rate of change at 700 hPa ≥ 1.45 K $(6\ \mathrm{h})^{-1}$	Synoptic speed at 700 hPa < 5 m s^{-1}
Wind direction	Wind blowing upvalley for at least 2 h between 0900 and 1900 LST + wind blowing downvalley most of the period between 0000 and 0800 LST	10-m wind direction from the expected sector with a min duration of 3 h	
Rainfall		Daily rainfall accumulation < 0.5 mm	

favorable days an inspection of observed wind direction, to make sure that the observed value is consistent with the one expected on the basis of topography.

On the contrary, here we propose a criterion based on ambient conditions, which does not include any requirement on the wind direction (see Table 2). As such, it can be used for preliminary screening of extended datasets, to filter out days that are unlikely to allow for slope winds. Furthermore, the criterion has been specifically devised for detecting upslope winds, whose complete and clean development is in general more difficult to detect than for their nocturnal counterpart. Indeed, upslope winds are prone to include thermal convection: hence flow patterns do not always follow closely the terrain. Instead, drainage winds are usually associated with strong stability and, as such, constrained to flow closely following the local topography. To sum up, the present criterion for the identification of slope wind days differs from those proposed in the literature to detect valley wind days, as it includes significantly different requirements both on radiation and synoptic conditions.

The two criteria proposed by Giovannini et al. (2017) and Román-Cascón et al. (2019) have been preliminarily tested on the present dataset to identify slope wind days, that is, days during which the entire cycle of up and downslope winds is fully developed and observed. A first visual check of selected days revealed that a significant part of them was not associated with pure slope circulations. This suggested that the test is probably not enough restrictive on the "weak" synoptic forcing, a condition required to prevent weather factors from interfering with the "clean" development of a pure upslope flow during daytime. Indeed, slope and valley wind systems do share some fundamental characteristics, but the specific time and spatial scales of their development are quite different. Accordingly, also their response to changes in the external forcing may be quite different, even under the same

environmental conditions. As explained in Table 2, the criterion proposed here restricts the conditions on radiation suggested by Giovannini et al. (2017) to exclude even days when sporadic convective clouds may temporarily shade the terrain, and hence cause intermittencies in the surface heat flux. Moreover, it restricts the condition on the synoptic forcing proposed by Román-Cascón et al. (2019) to remove the effect of large-scale circulations. As the resulting criterion is more demanding, the number of selected days is smaller than the two criteria from the literature would allow. Indeed, 7 days were identified in the spring season [vs 19 from Giovannini et al. (2017) and 16 from Román-Cascón et al. (2019)] and 6 days in the autumn season (vs 16 and 21 days, respectively). These 13 cases were further individually inspected to make sure that in each case the wind direction was steadily downslope before the transition and upslope after. Based on this final criterion, 5 days were selected exhibiting clear and fully developed downslope and upslope wind phases: 29 September, 14 and 18 October 2012, and 2 and 16 May 2013. These cases will be identified throughout the paper as fall (i.e., autumn) (F1, F2, and F3) and spring (S1 and S2) cases, respectively as

TABLE 3. Duration of the morning transition in the case studies considered. The duration was computed following the method described in the text. The names used for the case studies are reported in the first column: F1, F2, and F3 refer to the fall cases, and S1 and S2 refer to the spring cases.

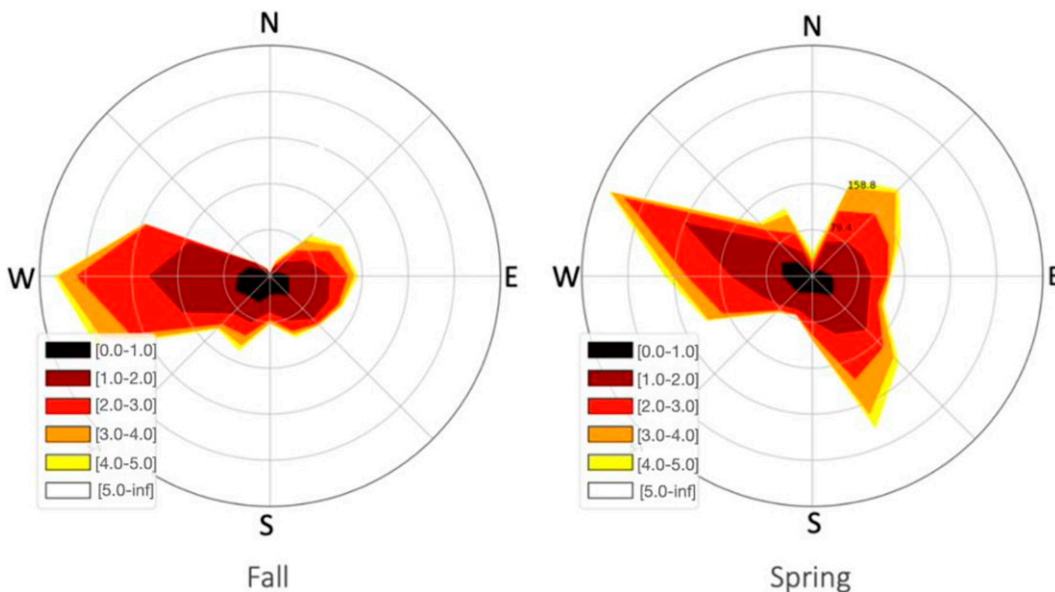|	Day	Length
F1	29 Sep	60 min
F2	14 Oct	58 min
F3	18 Oct	45 min
S1	2 May	15 min
S2	16 May	18 min

FIG. 3. Wind roses for the entire measurement period in (left) fall 2012 and (right) spring 2013. Analyzed data were collected at tower ES5 and averaged over 15 min. The downslope winds can be identified with a direction of ~270°, and the upslope winds have a direction of ~90°. The color scale indicates wind strength ranges (m s^{-1}), and the circles refer to 10% intervals of the entire set of values.

summarized also in Table 3. The extremely small number of days with a very clean development of morning and night regimes of slope winds is due to the peculiar characteristics of the measurement site, with the slope being part of an almost isolated massif and hence prone to perturbations from unevenly distributed surface forcing. These characteristics can be easily seen from the seasonal wind roses (Fig. 3) based on 15-min averaged data over the entire dataset from the tower ES5. ES5 was adopted as a reference as measurements taken there make it possible to detect more cleanly the two regimes as compared with all of the others. Considering the layout of the massif and the orientation of its slope, easterly winds correspond to upslope flows and westerly to downslope. Figure 3 shows that in both seasons the downslope phase is well defined and can be easily recognized, whereas the upslope component is less frequently observed. Also, signs of more significant synoptic disturbances in the spring component of the dataset are observed: a consistent part of the observed directions is different from the pure up and downslope ones.

b. Description of the case studies through the main meteorological variables

As a result of the above selection, all the cases exhibit high pressure, clear-sky conditions, and no synoptic disturbances, and share similar local-scale dynamics. Hence, for the sake of conciseness, we will describe in detail here only the dynamics of a single case (F3), as representative of the overall characteristics of katabatic and anabatic wind regimes. The time evolution of 5-min averaged values of wind direction and intensity is shown in Fig. 4. The upslope and downslope regimes are identified by the directions of 270° and 90°, respectively, and are clearly separated by two transitional phases, in the

morning and in the evening. Morning and evening transitions do not begin until sunrise and sunset have respectively occurred. The intensity of the along slope wind increases in time starting from the morning transition, after a transient calm
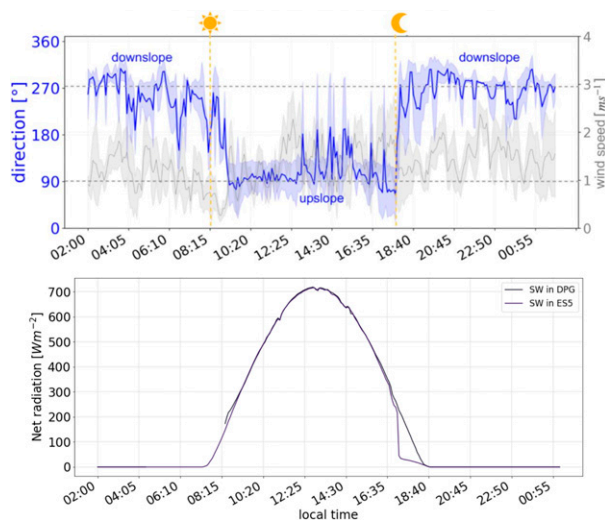

FIG. 4. Time evolution of the average (top) wind direction and speed and (bottom) incoming shortwave radiation during the case F3. For the wind data, the average value is computed using data collected at all towers ES2–ES5, and the associated error (gray band) is identified through the standard deviation. The two vertical dashed lines identify the times of local sunrise and sunset. Data (nondetrended) are averaged over 5 min, and the time in the x axis is local time (MDT). For the radiation data, the two lines refer to the radiation data collected at the highest measurement point on the slope (tower ES5) and on the valley floor (DPG).
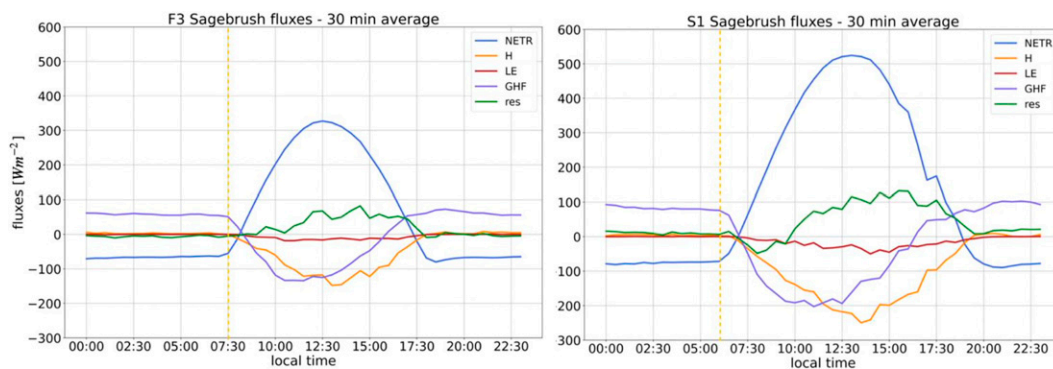
FIG. 5. Time evolution of the SEB for F2 and S1 from 0000 to 00000 local time. Different colors identify the different components, and the yellow vertical line indicates sunrise. The legend shows the identification of each component: H = sensible heat flux, LE = the latent heat flux, GHF = the ground heat flux, NETR = the net radiation, and res = the residual.

period (similarly to what was observed by Nadeau et al. 2013), and reaches its highest values during midmorning [as already observed by Whiteman et al. (2004) and Nadeau et al. (2013)]. The nighttime drainage flow is characterized by a periodic component due to the formation of gravity waves [already observed in this dataset by Lehner et al. (2015)], while the diurnal upslope wind is particularly steady for the first hours, whereas later presents some deviations from the purely along-slope direction, which may be determined by different factors (such as changing cloud cover, as observed in the radiometers data, dynamical forcing from upper synoptic-scale winds).

The SEB displays similar characteristics in all the selected cases. Hence their main features may be outlined describing two representative cases only, one in fall (F3) and one in spring (S1), as shown in Fig. 5. The observed seasonal variability of the energy balance is linked to several factors, for example, the sun elevation angle and the state of the vegetative cover (Matzinger et al. 2003; Wohlfahrt et al. 2016).The larger seasonal difference can be ascribed to the net radiation maxima: during spring the net radiation peaks at almost 500 W m^{-2} whereas in the fall cases the highest values are around 350 W m^{-2}. In both cases the residual component is close to 100 W m^{-2}. The main reason is that, in spring, not only net radiation amounts but also the latent heat fluxes are typically larger. These residuals persist throughout the days and imply the nonclosure of the surface energy budget, as already observed at the MATERHORN experiment site (Hang et al. 2016; Massey et al. 2017). Advection terms, both in the surface-normal and in the along-slope component, were also computed, but their values were too small to represent significative terms in the balance. Nevertheless, we can argue that these SEBs encompass suitable conditions for the development of slope winds, as the sensible heat flux is a largely prominent component of the budget (Whiteman 2000; Hoch and Whiteman 2010).

c. Characterization of the morning transition

The simplest way to identify the morning transition considers the reversal of the wind direction from down to upslope.

Other criteria look at the sign reversal of latent and sensible heat fluxes, as well as of the surface net radiation. The transition is also characterized by very low values of wind speed, which enable use of wind speed as an identification factor. The different estimates of the duration of the transition obtained for the same day from these different methods were compared, and the method based on direction was adopted as the most objective among all to detect the turning of the wind. The resulting duration of the morning transition for all five cases is shown in Table 3. It exhibits a large variability, in line with findings from Papadopoulos and Helmis (1999).

A seasonal variability is also observed, with a shorter duration of the transition during spring (10–15 min) than during fall (45–60 min). Differently from the observations reported in Nadeau et al. (2020), where the morning transition started approximately 40–50 min after sunrise, here the transition begins with the change of sign (from negative to positive) of the net radiation, which usually occurs less than 30 min after sunrise. In Fig. 6 the reference case study is used to highlight this characteristic: the 5-min-averaged values of all the levels of each tower (from ES1 to ES5) are represented along with the time evolution of the net and shortwave radiation in Fig. 6a, while an expanded view on the different levels of a single tower (ES3) is shown in Fig. 6b.

The mechanisms controlling the morning transition are affected both by the topography and by the nonuniform surface heating experienced by the sloping terrain at different times. A remarkable feature, emerging in all the case studies, is the propagation of the transition both along the slope and in the slope-normal direction. A time lag is observed among couples of consecutive towers, on the order of 10–15 min in fall and 5 min in spring. Clearly, the transition may be accompanied by other concurring or secondary phenomena, such as secondary flows associated with the local (nonideal) topographic features. Nevertheless, a clearly emerging feature is that the tower located on the valley floor (ES1) experiences the transition almost two hours later than all the other towers along the slope. This is consistent with the findings of Papadopoulos and Helmis (1999) and highlights how the alternating downslope–upslope diurnal
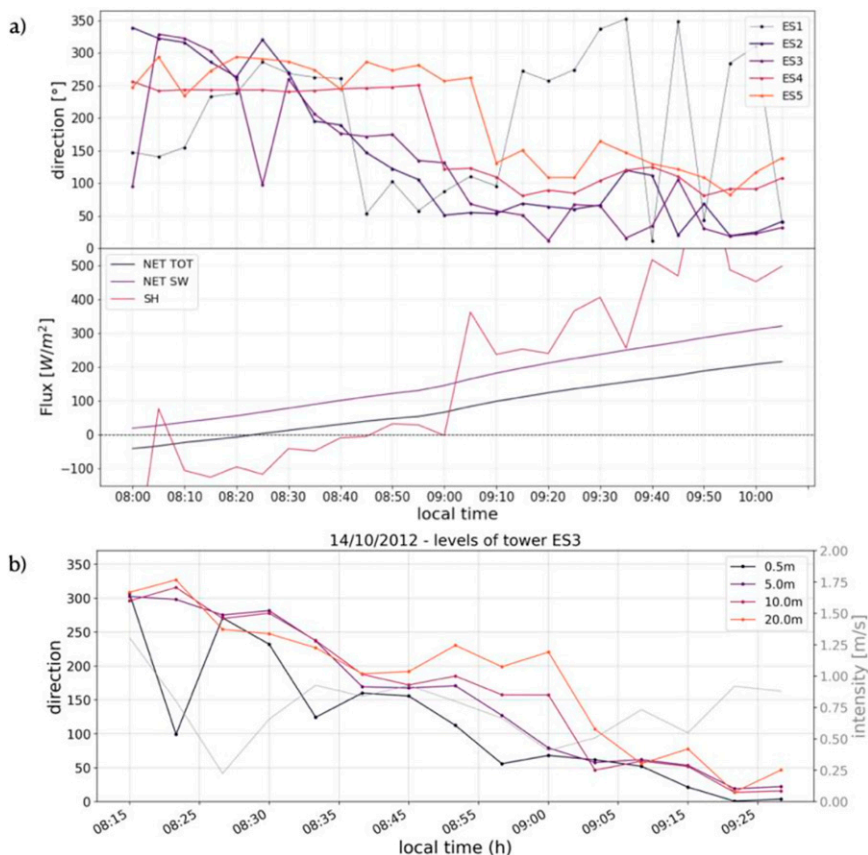
FIG. 6. Initiation of the transition on F3: (a) the scatterplot of the time evolution (MDT) of the averaged wind direction at each tower is reported, along with the evolution of both total and shortwave net radiation (notice that, as expected, ES1 behaves differently from all of the others, because it is located on the valley floor and not on the slope), and (b) the detail on the different levels of tower ES3.

cycle is a characteristic of the planetary boundary layer above the slope only, while the flow observed at the ES1 is mostly driven by the valley dynamics. For the vertical propagation of the transition initiation, it is found that the three lower levels evolve consistently and independently from the levels above 10 m.

d. Erosion of the nocturnal inversion at the foot of the slope

To fully understand the processes occurring along the slope after sunrise, it is also important to investigate the characteristics of the valley flow at the foot of the slope, and in particular, the mechanisms characterizing the erosion of the nighttime inversion at the valley experimental site, DPG. For this purpose, we analyzed all the available tethersonde profiles (for a total of 10 days) during both fall and spring campaigns: such an extensive dataset allowed a sounder statistical assessment of the erosion patterns envisaged by Whiteman (1982). At the same time, also including days in which the requirements for slope winds are not fulfilled does not invalidate the analysis, as far as the inversion breakup on the valley floor is to be characterized as such, rather than in its connections with slope winds. Note,

however, that these additional days are in any case characterized by unperturbed synoptic-scale conditions (as defined by Fernando et al. 2015). Once the erosion patterns are identified, the sole slope wind days are used to correlate nocturnal erosion to morning-transition processes.

1) STATISTICS AND IDENTIFICATION OF THREE MAIN PATTERNS

The main quantities characterizing the erosion processes, such as the inversion strength and height, and the time required to complete the erosion, are reported in Table 4. The different scenarios were classified considering case by case and not using an algorithm. High variability is found in the inversion height, as well as in the time required to complete the erosion, but no clear seasonality is observed.

Each transition event exhibits very closely one of the patterns identified by Whiteman (1982). In Fig. 7 one example for each pattern is reported in terms of subsequent vertical temperature profiles. Symbols indicate the inversion top estimated as the point where the lapse rate changes. Based on the documents accompanying the dataset, the height of each measurement point in the

TABLE 4. Summary of the main quantities characterizing the erosion processes: inversion ("Inv") strength, inversion height, erosion duration, and time of the beginning of the erosion for each day with available tethersonde measurements, together with the identified pattern and the erosion time computed using the thermodynamical model proposed by Whiteman and McKee (1982).

Case study	Day	Inv strength (K)	Inv height (m)	Erosion time: data	Beginning (LT)	Pattern	Erosion time: model
S1	2 May	7	50	2 h 15 min	0624	1	2 h 20 min
	12 May	12	100	Missing data	0612	2	—
S2	16 May	9	125	2 h 10 min	0608	3	2 h 20 min
	21 May	7	70	1 h 30 min	0604	1	1 h 40 min
	2 Oct	10	165	1 h 55 min	0725	3	2 h 5 min
F2	14 Oct	9	70	2 h 50 min	0738	3	2 h 30 min
F3	18 Oct	10	120	2 h 30 min	0742	2	2 h 30 min
F1	29 Sep	8	90	Missing data	0755	2	—
	26 May	3.5	60	Missing data	0611	3	—
	26 Sep	8	85	2 h 20 min	0719	3	2 h 50 min

sounding is accurate within ±1 m. The erosion pattern of S1 (Fig. 7a, pattern 1) is the most common over flat land (Whiteman 1982) and is characterized by a prevailing upward growth of a convective boundary layer from the ground due to the surface heating following sunrise. The inversion is eroded in

approximately 90 min. The erosion pattern of F3 (Fig. 7b, pattern 2) provides evidence of the opposite process: the descent of the inversion top from above. This behavior is generally associated in the literature with a higher reflectivity of the ground to incoming shortwave radiation, due to wet or
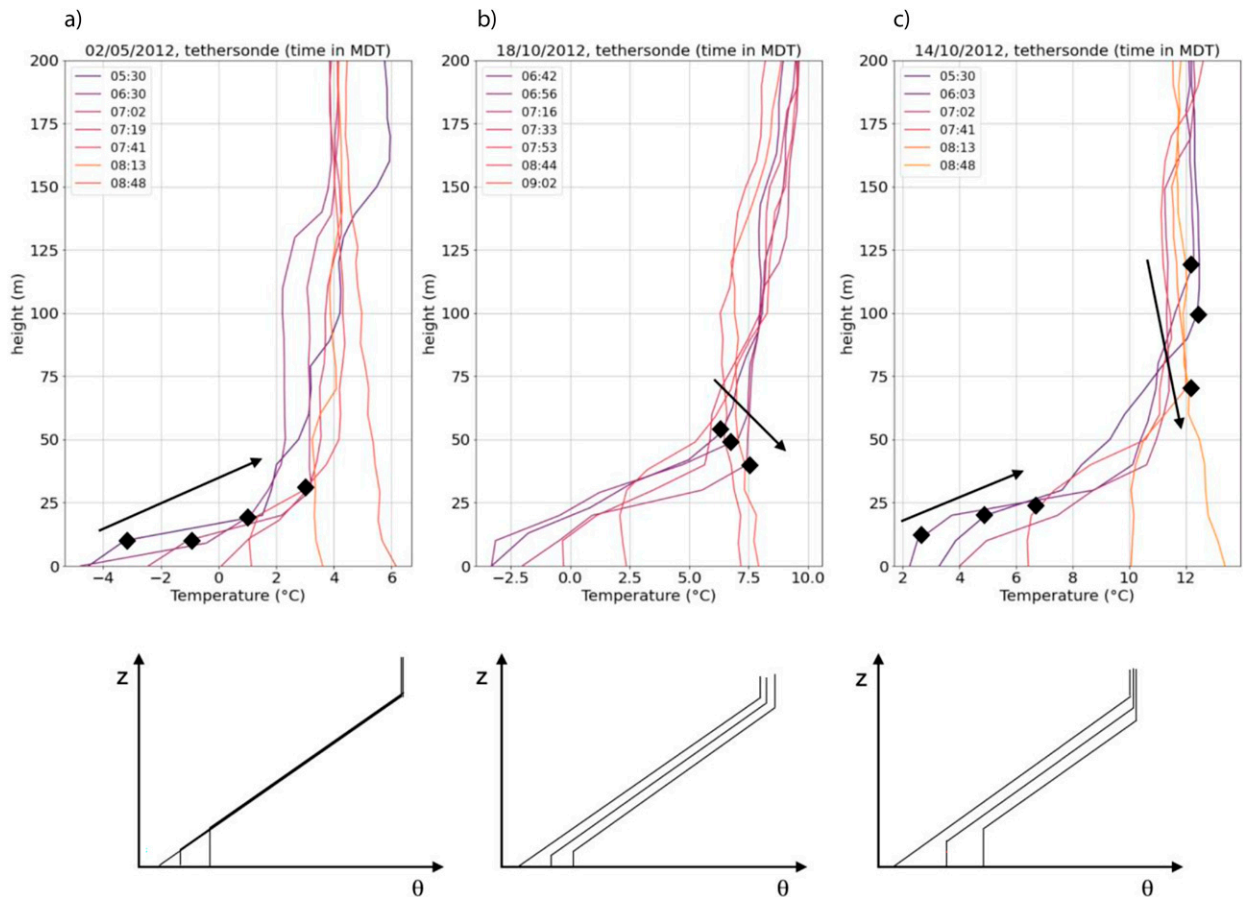

FIG. 7. Examples of patterns of the inversion erosion: (a) upward growth of the CBL, (b) descent of the inversion top, and (c) a mix of the two previous patterns. The three plots represent the time evolution of the vertical temperature profile measured by tethersonde launched from the Sagebrush site. Each line refers to an ascent, identified by the launching time reported in the legend. Data refer to the mornings of S1 [in (a)], F3 [in (b)], and F2 [in (c)], which are also the selected cases for the observation of the upslope winds. A schematic representation of the three patterns is represented below each plot.

icy terrain (Whiteman 1982). Indeed, for the present cases, this situation was confirmed by further investigations on data from either radar or weather stations in the valley, reporting precipitation events during the evening and night before (not shown). The erosion pattern of F2 is a perfect example of the third and most common pattern in the dataset (with 6 of 10 cases), consisting in the combination of the two previous processes. Indeed, both the growth of the convective boundary layer from below and the descent of the inversion top can be observed.

The model proposed by Whiteman and McKee (1982) is not fully suited for the present case, for different reasons, including the differences in the geometry of the problem and the poor representation of the wind structure. However, the model can be used at least as a proxy scheme for understanding the basic mechanisms implied in the transition and to discriminate different transition scenarios. Of course, further insights can only be obtained from more sophisticated modeling. Indeed, numerical simulations of daytime thermally driven winds over a plain-slope configuration performed by De Wekker (2008) show a depression of the mixed layer at the basis of the mountain slope, which is thought to be caused by subsidence in the return branch of the upslope flow (De Wekker 2008; Serafin and Zardi 2010). This evidence suggests that the mechanisms governing the transition are still controlled by phenomena occurring in the vicinity of the slope basis, and not at the entire valley or plain level. This also shows that the mass conservation is not the main driving constraint in this case, but other conservation principles (of momentum and energy) play a role too. However, no analytical model proposed so far can capture these mechanisms and the identification of a new one is beyond the scope of this work. So, we are going to use the Whiteman–McKee model using an "effective" valley width to represent the fact that the subsidence induced by the upslope flow and continuity is confined within a limited distance downwind (with respect to the upper-level flow) from the ridge top.

The classification of the erosion processes in different patterns is summarized in Table 4. The most common mechanism observed among the 10 cases analyzed is the third one, that is, the descent of the inversion top followed by the upward growth of the CBL. Indeed, 6 of 10 erosion patterns can be attributed to this mechanism, and most of them occur during falls. The second mechanism is observed only in two cases, and it requires particularly high values of albedo (as outlined above), whereas the first mechanism appears to be the least observed one. In the case studies associated with the third mechanism, some interesting features were observed before the onset of the erosion: the radiation recorded on the previous day suggests the presence of clouds in the afternoon, following clear-sky conditions in the morning before; the relative humidity measured from the valley tower (ES1) during the night reaches high values (70%–80%) during the hours before sunrise; finally, temperature exhibits on average an increasing trend during the previous days. From these observations the descent of the inversion top appears to be a feature common to most of the case studies, despite it is usually considered a typical characteristic of deep and narrow valleys.

2) COMPARISON OF DATA WITH THE THERMODYNAMICAL MODEL BY WHITEMAN AND MCKEE (1982)

The Whiteman and McKee (1982) model, adopting the heuristic approach anticipated above, is used as a proxy for guiding our investigation of the basic mechanisms implied in the transition of slope winds, that is, the top-down erosion and the growth from the ground. Indeed, although originally conceived for deep valleys, it makes it possible to reproduce fairly well the observed subsidence in all the three identified patterns, upon appropriate settings of surface energy partitioning and a suitable choice of an effective valley width. Fig. 8 shows the schematization of the topography and the definition of the main geometric parameters used in the model.

The model is based on two equations prescribing the dependence of the growth rate of the CBL depth and the rate of descent of the inversion top on inversion characteristics, incoming energy, and valley topography:

$$\frac{dH}{dt} = \frac{\theta}{T}\frac{k}{\rho c_p}\left[\frac{l + HC}{l + (1/2)HC}\right]\frac{A_0 A_1}{\gamma H}\,\sin\left[\frac{\pi}{\tau}(t - t_i)\right]\text{ and}$$

$$\frac{dh}{dt} = -\frac{\theta}{T}\frac{1}{\rho c_p}\left[\frac{l + hC - k(l + HC)}{l + (1/2)HC}\right]\frac{A_0 A_1}{\gamma h}\,\sin\left[\frac{\pi}{\tau}(t - t_i)\right],$$

where h is the height of the inversion top, H is the height of the CBL, $C = 1/\tan\alpha_1 + 1/\tan\alpha_2$ is a function of the sidewall slope angles α_1 and α_2, A_0 is the fraction of the solar energy flux that is transferred into the valley, A_1 is the amplitude of the sinusoidal function representing the incoming solar radiation, τ is its period, γ is the potential temperature gradient in the stable core, l is the width of the valley floor, and k describes the fraction of energy used for the CBL growth. In the model, k is a number between 0 and 1, and it is a fundamental parameter because it determines the development of one pattern or the other through the regulation of the energy partitioning; indeed, the fraction of energy used to drive the CBL growth is given by $k[(l + HC)/(l + hC)]$.

Figure 9 shows the erosion mechanisms reproduced by the above thermodynamical model. Observed values from soundings are compared with those predicted by the model in terms of the height of the convective boundary layer H, the inversion top h, and the vertical temperature profile. The three cases can be identified in the three panels: the growth of the CBL from below through an increasing H (Fig. 9a), the descent of the inversion top through decreasing values of h (Fig. 9b), and a combination of the two mechanisms through the opposite trends observed for H and h in time (Fig. 9c). The pattern in Fig. 9a is obtained with $k = 1$, that is, assuming that the entire fraction of energy entering the area topping the valley is used to feed the growth of the CBL, whereas the pattern in Fig. 9b is associated with $k = 0.1$, that is, assuming that (most of) the energy available for the erosion contributes to promoting the airflow along the sidewalls, causing the top of the inversion to descend. The pattern in Fig. 9c results from intermediate values among these two extremes. In the last column of Table 3, a comparison between the observed time needed to complete the erosion and the one derived from the thermodynamical model is shown.
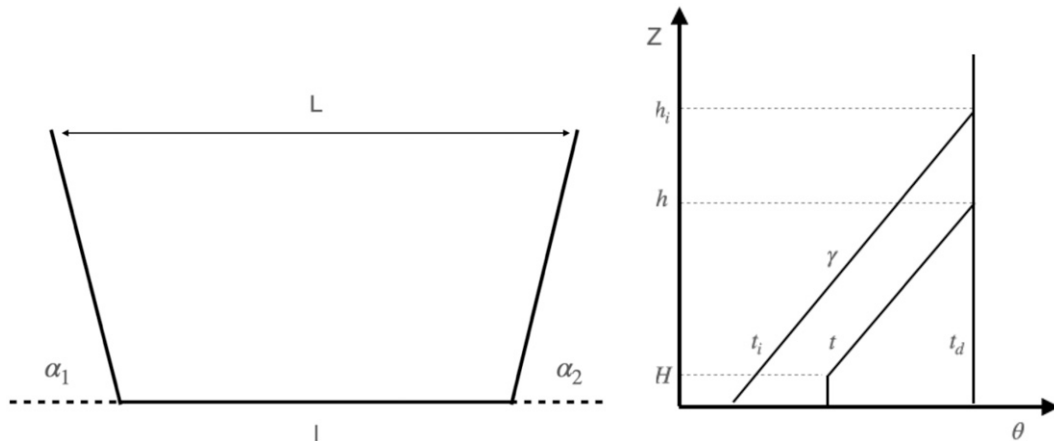
FIG. 8. (left) Valley geometry and (right) potential temperature profile evolution in the Whiteman and McKee (1982) model. The geometrical characteristics of the valley and the temperature profiles are described by introducing the variables represented in the figure, which are then used in the model equations.

The width of the valley, in the model, was set equal to 6.0 km, which is the distance from the slope to the DPG site, in the valley, where the observed dynamic is that of a valley wind. The reproducibility of the observed patterns supports the hypothesis, stated at the beginning of the section, on the suitability of Whiteman's (1982) model as far as the processes are controlled by phenomena occurring in the vicinity of the slope base.

The occurrence of a specific pattern is clearly linked to the topographic characteristics of the valley, resulting in the prevalence of the upward growth of the CBL in broad valleys, whereas the descent of the inversion top characterizes cases in deep valleys (Whiteman and McKee 1982). In the following section, we will discuss how different meteorological factors lead to the predominance of one specific process.

4. Discussion

The main mechanisms driving the transition from nighttime downslope winds to daytime upslope winds over Granite

Mountain (Utah), an isolated mountain facing a broad valley, were investigated on the basis of data from observations during intensive field measurements, in connection with the breakup of nighttime temperature inversion. Patterns in the process of inversion breakup were identified from the analysis of vertical temperature profiles taken over the valley floor and associated with the main processes controlling the morning transition over the slope. To categorize the different mechanisms, two cases (S1 and S2) were analyzed using data collected at the towers installed along the slope for the identification of the transition process and from the tethersonde to identify the erosion process. The three patterns proposed in Whiteman (1982) and recalled above will be used as a guidance for categorizing the events.

The erosion process observed during episode S2 is characterized by a "type c" pattern: the reversal of the slope wind begins in the upper part of the slope (ES5), about 5 min before affecting the lower part (bottom panel in Fig. 10). A possible explanation for the observed phenomena is that the heating of the air above the slope starts from the upper part
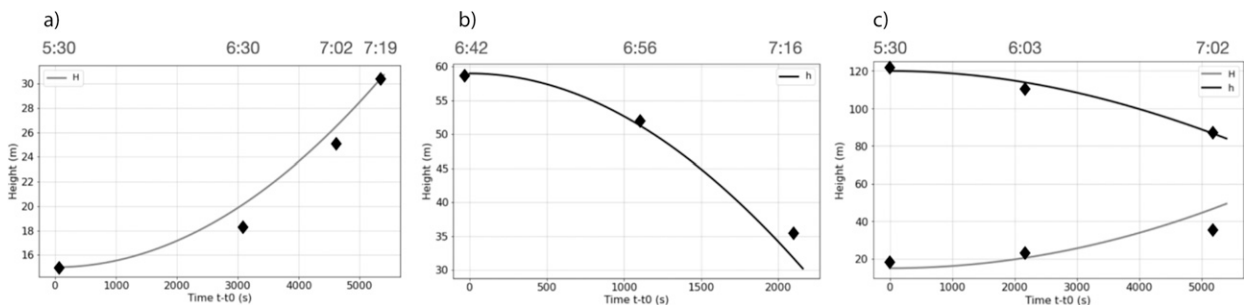

FIG. 9. Comparison between data from observations and results from the thermodynamical model proposed by Whiteman and McKee (1982). The height of the growing convective boundary layer H and the height of the descending inversion top h resulting from the thermodynamical model (solid lines) are represented as a function of time from the beginning of the process (at $t = t_0$). Shown are (a) episode S1, (b) episode F3, and (c) episode F2, and they are compared with the time evolution of the vertical profiles of temperature shown in Fig. 7 (diamonds). The values of the model parameters are $\alpha_1 = 6°$, $\alpha_2 = 10°$, $l = 6.0$ km, and A1 = 300, with γ, k, and A_0 varying according to the case study.
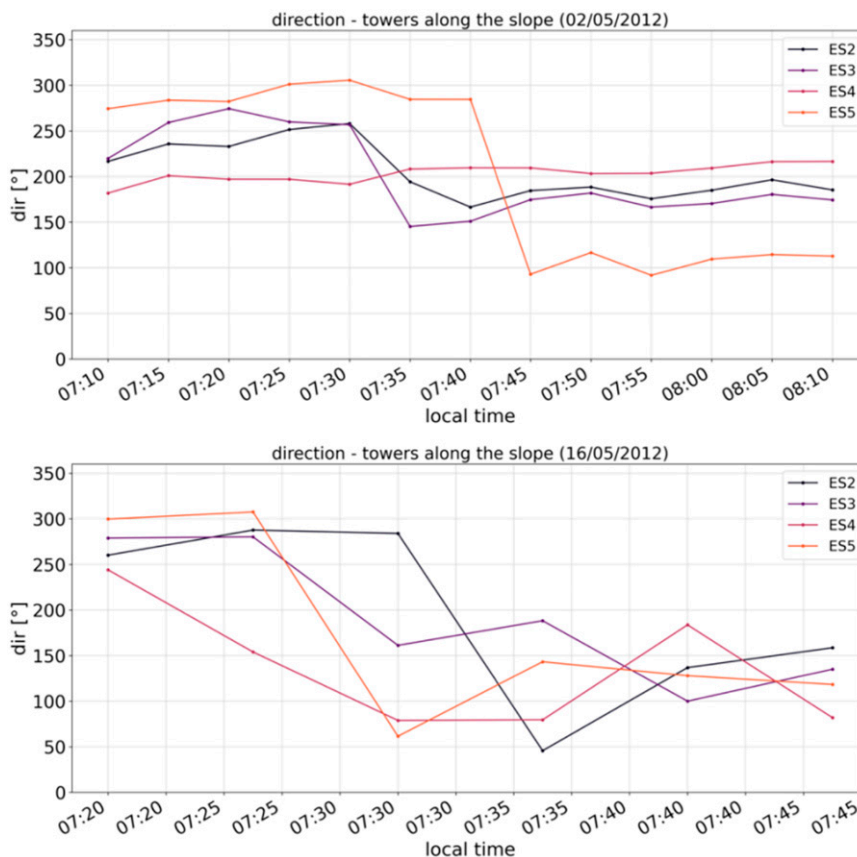
FIG. 10. Expanded view of the evolution of the average wind direction measured at different towers along the slope during two cases taken as examples, (top) S1 and (bottom) S2. Different lines refer to different towers (ES2–ES5) as indicated in the legend. Time on the *x* axis is local time, and data are averaged over 5-min time windows.

of the slope and is promoted by the turbulent exchange. This heating drives the setup of an upslope flow that, through advection, ends up characterizing the entire slope. The removal of air from the lower part of the slope-valley atmosphere leads to the descent of the inversion top, which is observed in the tethered balloon soundings. With increasing incoming radiation, the surface heating increases in turn, and the erosion continues with a combination of the two processes. When the initiation of the morning transition is driven by top-down heating from turbulent exchanges with upper air, it starts in the higher part of the slope wind layer and subsequently covers the entire slope length, driven by turbulent mixing. This process leads to the descent of the top inversion in the valley's vertical structure.

In the breakdown of the nocturnal inversion during the first hours of episode S1, it is very evident the primary role of the convective boundary layer growth from the surface, starting right after sunrise [at 0630 mountain daylight time (MDT)]. Instead, the wind reversal associated with the morning transition starts at the foot of the slope (as observed at ES2 and ES3), and then propagates upward to the slope top, as observed in the top panel of Fig. 10. When the erosion of the nocturnal inversion is mainly driven by the upward growth of

the CBL, the morning transition is promoted by the heating of the overlying air from the surface, and the wind reversal starts in the lower part of the slope.

The factors leading to the development of one pattern of transition rather than another are to be found in the surface energy budgets. The comparison between the turbulent heat fluxes on the valley floor (DPG site) and on the slope (ES3 tower) is shown in Fig. 11.

In the case of S1, a clear delay in the reversal of the sensible heat flux between the valley floor and the slope is observed (highlighted in Fig. 11a with black arrows). The stronger sensible heat flux on the slope determines the initiation of the upslope flow in the upper part of the slope. Hence, by removing air from higher levels, it extends rapidly over the entire slope and stops the growth of the convective boundary layer at the foot. On the other hand, when the two fluxes are comparable, the convective boundary layer grows from the valley floor: the upslope flow develops initially in the lower part of the slope and then expands to its entirety.

A simple schematization of these two processes is shown in Fig. 12, where the relative magnitudes of the heat fluxes in the valley or along the slope are represented by the dimension of the black arrows, and the development of the
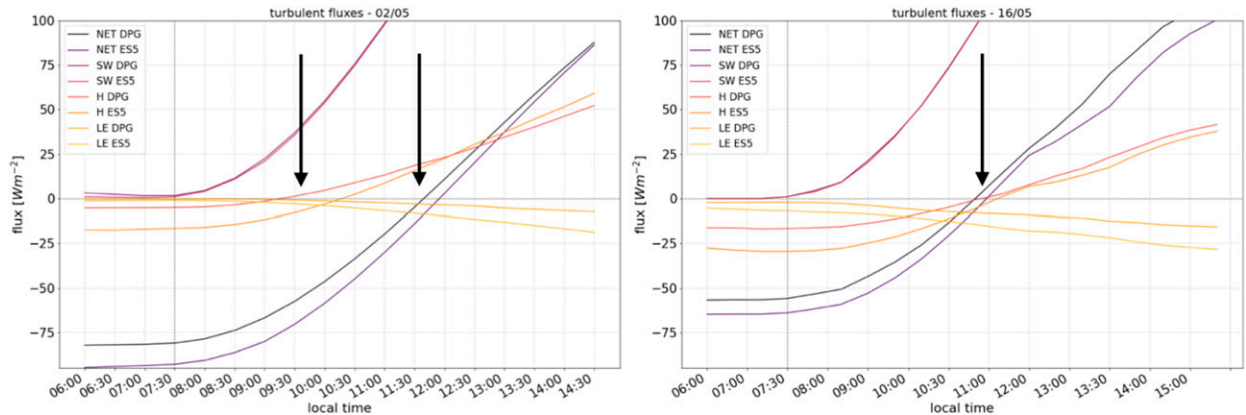
FIG. 11. Time series of energy fluxes on the valley floor (DPG site) and the slope (ES5 site) for two selected cases, (left) S1 and (right) S2, in a period centered at sunrise. The vertical dashed line represents local sunrise, and the black arrow highlights the differences between the two cases. The labels in the legend indicate the net radiation (NET), sensible heat flux (SH), and latent heat flux (LE).

upslope flow is identified with the orange arrows. The upward growth of the convective boundary layer, represented in Fig. 12b, is associated with the stronger sensible heat flux in the valley floor, while the development of upslope flows at higher levels over the slope, as well as the subsequent mass removal, is associated with the stronger sensible heat flux on the slope. The descent of the inversion, represented in Fig. 12a, is instead linked to a sensible heat flux that is stronger on the slope and hence determines stronger upslope flows, as is found in observations (with a difference of 0.8–1.0 m s^{-1}).

5. Conclusions

Data from high-resolution measurements of wind and temperature collected within the MATERHORN Program at the experimental site of Dugway Proving Ground (Utah) were analyzed to identify the transition processes characterizing the diurnal cycle of slope winds over the east-facing slope of Granite Mountain.

A criterion for the identification of slope wind days (i.e., days during which the entire cycle of up- and downslope winds is likely to be observed) was outlined and tested on the extensive MATERHORN dataset to select the case studies to be examined. The criterion differs from others available in the literature for the identification of valley wind days (i.e., days during which the entire cycle of up- and downvalley winds is observed). This is consistent with the smaller response times and higher sensitivity to ambient conditions and to the regularity of incoming radiation that slope wind systems exhibit, in comparison with valley wind systems. To the best of the author's knowledge, the proposed criterion is the first of
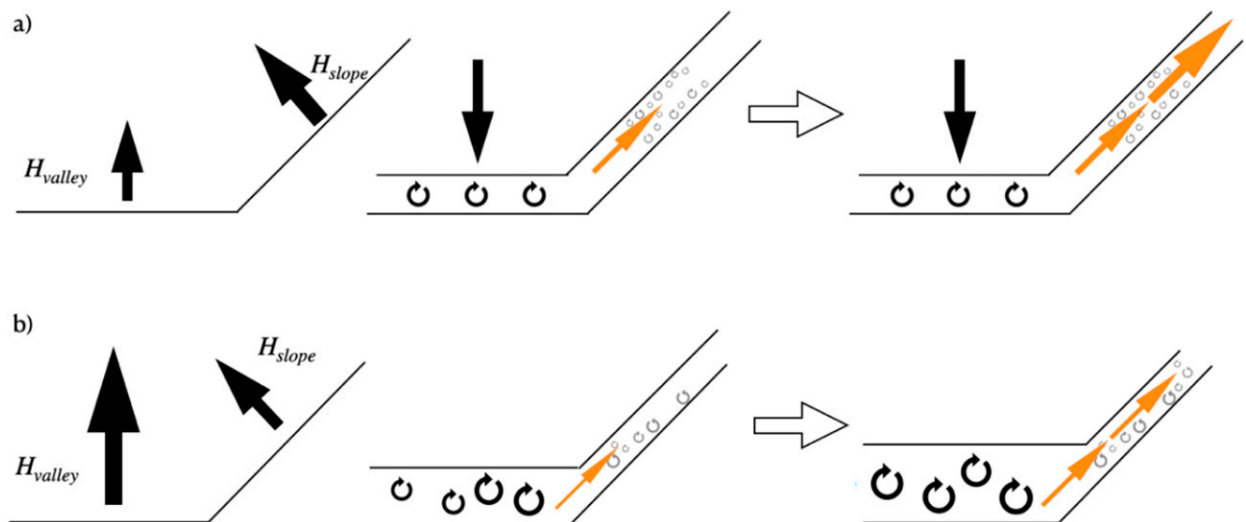

FIG. 12. Schematization of the morning transition and erosion of the nocturnal inversion processes, showing the two possible mechanisms of erosion (b) from below (due to surface heating) or (a) from above (due to mixing). Notice that the role of sensible heat is also represented.

its kind, as no other criteria are available in the literature specifically conceived for slope winds.

The morning transition from katabatic to anabatic flow was characterized by an almost unique configuration represented by an east-facing gentle slope of an almost isolated massif facing a wide-open valley. Data for the analysis were taken from multiple sources along the slope during two different seasons (with the seasonality being an opportunity almost exclusively granted by the specific choice of the MATERHORN dataset).

Very few studies have been so far specifically dedicated to the characterization of the morning transition in the field, and those available mostly deal with steep slopes in narrow valleys. Among the most interesting properties of the transition, a seasonal dependence of its duration was found: the transitions are more rapid during the spring than in the autumn cases ($\sim$10 vs $\sim$60 min). Also, it is very evident the propagation of the reversal, both along the slope and in the vertical direction, the latter reminiscent of a feature observed in the analytical model proposed by Zardi and Serafin (2015). The change of sign of the total radiation identifies the beginning of the transition.

The mechanisms of erosion of the nocturnal inversion in the valley at the foot of the slope were identified, and the erosion processes were classified following the three patterns outlined by Whiteman (1982). Different patterns are usually linked to the different topographical configurations of the valleys, both in terms of experimental observations (Kuwagata and Kimura 1995; Whiteman et al. 2004; Brehm and Freytag 1982; Banta and Cotton 1981) and mathematical modeling (Whiteman and McKee 1982; Zoumakis and Efstathiou 2006a,b), have been observed also in the Granite Mountain site and linked to the environmental conditions, rather than to the geometry of the valley. The occurrence of either pattern is determined by the partitioning of the energy available from incoming radiation. This energy may be spent either for the CBL growth or for setting the airflow in motion up the slope, as confirmed by comparison with the thermodynamical model (Whiteman and McKee 1982).

Three possible mechanisms driving the morning transition over the slope and the process of erosion of the inversion at the foot of the slope were connected here for the first time. The occurrence of each erosion pattern is found to be associated with of a specific pattern of transition: in particular, when the reversal is governed by the heating through turbulent mixing with upper air, the transition from katabatic to anabatic flows starts in the higher part of the slope and removes air from the valley core, leading to the descent of the inversion top for mass conservation. This situation is observed to occur when the reflectivity of the terrain is larger than usual, especially because of recent precipitation as identified through the large values of relative humidity within the valley before the onset of the transition. On the contrary, when the prevailing mechanism is governed by surface heating, the destruction of the katabatic layer starts from the lower levels and propagates upward, while the nocturnal inversion is eroded by the onset and evolution of a convective boundary layer at the surface.

The key factor that determines the development of one of these two processes is the ratio between the surface turbulent fluxes of sensible heat, as schematized in Fig. 12. A sensible heat flux higher on the slope than in the valley determines the development of an upslope flow in the upper part of the slope removing air and thus promoting the descent of the inversion top, while the opposite condition allows the CBL growth from the valley floor. The hypothesized role of sensible heat is confirmed by data concerning the surface energy budget and by the different trends observed in their values in connection with the different patterns observed in the selected case studies.

The unprecedented deployment of instrumentation characterizing the MATERHORN campaigns, which made the resulting dataset possibly superior to any other available dataset for the purpose of the present case study, made it possible to investigate in detail the spatial and temporal structure of the phenomena of interest. Nevertheless, further experimental campaigns, more specifically focusing on slope winds, would be desirable to pursue further the analysis on aspects that were not fully detected here and make progress with our understanding of slope flows, especially anabatic winds. In particular, to avoid any interference from other topographic factors, a close-to-idealized slope would be required, with the extensive deployment of instrumentation both along the vertical and the horizontal direction, and with finer data collection during daytime. Further understanding of the mechanism driving the transition from katabatic to anabatic winds on a slope could be obtained through measurements over slopes more suitable for a clean and undisturbed development of this kind of circulation (i.e., steeper slopes). Also, the sensitivity of the observed patterns on different surface properties and on different seasons should be further investigated as well.

Future research efforts should certainly explore the analysis of turbulence in the slope layer during the transitional period and the daytime regime, which appears to be the natural continuation of this work. To this purpose, a unique opportunity is offered by the ongoing cooperative research program Multi-Scale Transport and Exchange Processes in the Atmosphere over Mountains (TEAMx), which is pursuing the goal of the exploration of transport and exchange processes in mountainous areas at different scales, using a combined approach of intensive field measurements and high-resolution numerical modeling (Serafin et al. 2018, 2020; Rotach et al. 2022).

from the MATERHORN experiment and to Dr. Carlos Román-Cascón for fruitful discussion and suggestions on the process of selecting days for study.

Data availability statement. All of the meteorological data created or used during this study are openly available from the Mountain Terrain Atmospheric Modeling and Observations (MATERHORN) Program repository, which can be found online (https://www.eol.ucar.edu/node/12006).

REFERENCES

Atkinson, B. W., 1981: *Mesoscale Atmospheric Circulations.* Academic Press, 495 pp.

Ayer, H. S., 1961: On the dissipation of drainage wind systems in valleys in morning hours. *J. Meteor.*, **18**, 560–563, https://doi.org/10.1175/1520-0469(1961)018<0560:OTDODW>2.0.CO;2.

Bader, D. C., and T. B. McKee, 1983: Dynamical model simulation of the morning boundary layer development in deep mountain valleys. *J. Climate Appl. Meteor.*, **22**, 341–351, https://doi.org/10.1175/1520-0450(1983)022<0341:DMSOTM>2.0.CO;2.

——, and ——, 1985: Effects of shear, stability and valley characteristics on the destruction of temperature inversions. *J. Climate Appl. Meteor.*, **24**, 822–832, https://doi.org/10.1175/1520-0450(1985)024<0822:EOSSAV>2.0.CO;2.

Banta, R. M., 1984: Daytime boundary layer evolution over mountainous terrain. Part I: Observations on the dry circulation. *Mon. Wea. Rev.*, **112**, 340–356, https://doi.org/10.1175/1520-0493(1984)112<0340:DBLEOM>2.0.CO;2.

——, 1986: Daytime boundary layer evolution over mountainous terrain. Part II: Numerical studies of upslope flow duration. *Mon. Wea. Rev.*, **114**, 1112–1130, https://doi.org/10.1175/1520-0493(1986)114<1112:DBLEOM>2.0.CO;2.

——, and W. R. Cotton, 1981: An analysis of the structure of local wind systems in a broad mountain basin. *J. Appl. Meteor.*, **20**, 1255–1266, https://doi.org/10.1175/1520-0450(1981)020<1255:AAOTSO>2.0.CO;2.

Barbano, F., L. Brogno, F. Tampieri, and S. Di Sabatino, 2022: Interaction between waves and turbulence within the nocturnal boundary layer. *Bound.-Layer Meteor.*, **183**, 35–65, https://doi.org/10.1007/s10546-021-00678-2.

Brazel, A. J., H. J. S. Fernando, J. C. R. Hunt, N. Selover, B. C. Hedquist, and E. Pardyjak, 2005: Evening transition observations in phoenix, Arizona. *J. Appl. Meteor.*, **44**, 99–112, https://doi.org/10.1175/JAM-2180.1.

Brehm, M., and C. Freytag, 1982: Erosion of the night-time thermal circulation in an alpine valley. *Arch. Meteor. Geophys. Bioclimatol.*, **31B**, 331–352, https://doi.org/10.1007/BF02263439.

Charrondière, C., C. Brun, J.-E. Sicart, J.-M. Cohard, R. Biron, and S. Blein, 2020: Buoyancy effects in the turbulence kinetic energy budget and Reynolds stress budget for a katabatic jet over a steep alpine slope. *Bound.-Layer Meteor.*, **177**, 97–122, https://doi.org/10.1007/s10546-020-00549-2.

——, ——, J.-M. Cohard, J.-E. Sicart, M. Obligado, R. Biron, C. Coulaud, and H. Guyard, 2022: Katabatic winds over steep slopes: Overview of a field experiment designed to investigate slope-normal velocity and near surface turbulence. *Bound.-Layer Meteor.*, **182**, 29–54, https://doi.org/10.1007/s10546-021-00644-y.

Chow, F. K., S. F. J. De Wekker, and B. J. Snyder, 2013: *Mountain Weather Research and Forecasting: Recent Progress and Current Challenges.* Springer, 760 pp.

Cintolesi, C., D. Di Santo, F. Barbano, and S. Di Sabatino, 2021: Anabatic flow along a uniformly heated slope studied through large-eddy simulation. *Atmosphere*, **12**, 850, https://doi.org/10.3390/atmos12070850.

Colette, A., F. K. Chow, and R. L. Street, 2003: A numerical study of inversion-layer breakup and the effects of topographic shading in idealized valleys. *J. Appl. Meteor.*, **42**, 1255–1272, https://doi.org/10.1175/1520-0450(2003)042<1255:ANSOIB>2.0.CO;2.

De Wekker, S. F. J., 2008: Observational and numerical evidence of depressed convective boundary layer heights near a mountain base. *J. Appl. Meteor. Climatol.*, **47**, 1017–1026, https://doi.org/10.1175/2007JAMC1651.1.

——, and M. Kossmann, 2015: Convective boundary layer heights over mountainous terrain—A review of concepts. *Front. Earth Sci.*, **3**, 77, https://doi.org/10.3389/feart.2015.00077.

——, ——, J. C. Knievel, L. Giovannini, E. D. Gutmann, and D. Zardi, 2018: Meteorological applications benefiting from an improved understanding of atmospheric exchange processes over mountains. *Atmosphere*, **9**, 371, https://doi.org/10.3390/atmos9100371.

Doran, J. C., and T. W. Horst, 1981: Velocity and temperature oscillations in drainage winds. *J. Appl. Meteor.*, **20**, 361–364, https://doi.org/10.1175/1520-0450(1981)020<0361:VATOID>2.0.CO;2.

——, and ——, 1983: Observations and models of simple nocturnal slope flows. *J. Atmos. Sci.*, **40**, 708–717, https://doi.org/10.1175/1520-0469(1983)040<0708:OAMOSN>2.0.CO;2.

Fernando, H. J. S., and Coauthors, 2015: The MATERHORN: Unraveling the intricacies of mountain weather. *Bull. Amer. Meteor. Soc.*, **96**, 1945–1967, https://doi.org/10.1175/BAMS-D-13-00131.1.

Freytag, C., 1987: Results from the MERKUR experiment: Mass budget and vertical motions in a large valley during mountain and valley wind. *Meteor. Atmos. Phys.*, **37**, 129–140, https://doi.org/10.1007/BF01040843.

Giovannini, L., L. Laiti, S. Serafin, and D. Zardi, 2017: The thermally driven diurnal wind system of the Adige Valley in the Italian Alps. *Quart. J. Roy. Meteor. Soc.*, **143**, 2389–2402, https://doi.org/10.1002/qj.3092.

——, E. Ferrero, T. Karl, M. W. Rotach, C. Staquet, S. Trini Castelli, and D. Zardi, 2020: Atmospheric pollutant dispersion over complex terrain: Challenges and needs for improving air quality measurements and modeling. *Atmosphere*, **11**, 646, https://doi.org/10.3390/atmos11060646.

Grachev, A. A., L. S. Leo, S. D. Sabatino, H. J. S. Fernando, E. R. Pardyjak, and C. W. Fairall, 2016: Structure of turbulence in katabatic flows below and above the wind-speed maximum. *Bound.-Layer Meteor.*, **159**, 469–494, https://doi.org/10.1007/s10546-015-0034-8.

Hang, C., D. F. Nadeau, D. D. Jensen, S. W. Hoch, and E. R. Pardyjak, 2016: Playa soil moisture and evaporation dynamics during the MATERHORN field program. *Bound.-Layer Meteor.*, **159**, 521–538, https://doi.org/10.1007/s10546-015-0058-0.

Hoch, S. W., and C. D. Whiteman, 2010: Topographic effects on the surface radiation balance in and around Arizona's meteor crater. *J. Appl. Meteor. Climatol.*, **49**, 1114–1128, https://doi.org/10.1175/2010JAMC2353.1.

Horst, T. W., and J. C. Doran, 1986: Nocturnal drainage flow on simple slopes. *Bound.-Layer Meteor.*, **34**, 263–286, https://doi.org/10.1007/BF00122382.

——, and ——, 1988: The turbulence structure of nocturnal slope flow. *J. Atmos. Sci.*, **45**, 605–616, https://doi.org/10.1175/1520-0469(1988)045<0605:TTSONS>2.0.CO;2.

Hunt, J. C. R., H. J. S. Fernando, and M. Princevac, 2003: Unsteady thermally driven flows on gentle slopes. *J. Atmos. Sci.*, **60**, 2169–2182, https://doi.org/10.1175/1520-0469(2003)060<2169:UTDFOG>2.0.CO;2.

Kossmann, M., R. Vögtlin, U. Corsmeier, B. Vogel, F. Fiedler, H.-J. Binder, N. Kalthoff, and F. Beyrich, 1998: Aspects of the convective boundary layer structure over complex terrain. *Atmos. Environ.*, **32**, 1323–1348, https://doi.org/10.1016/S1352-2310(97)00271-9.

Kuwagata, T., and J. Kondo, 1989: Observation and modeling of thermally induced upslope flow. *Bound.-Layer Meteor.*, **49**, 265–293, https://doi.org/10.1007/BF00120973.

——, and F. Kimura, 1995: Daytime boundary layer evolution in a deep valley. Part I: Observations in the Ina Valley. *J. Appl. Meteor.*, **34**, 1082–1091, https://doi.org/10.1175/1520-0450(1995)034<1082:DBLEIA>2.0.CO;2.

——, and ——, 1997: Daytime boundary layer evolution in a deep valley. Part II: Numerical simulation of the cross-valley circulation. *J. Appl. Meteor.*, **36**, 883–895, https://doi.org/10.1175/1520-0450(1997)036<0883:DBLEIA>2.0.CO;2.

Lehner, M., and M. W. Rotach, 2018: Current challenges in understanding and predicting transport and exchange in the atmosphere over mountainous terrain. *Atmosphere*, **9**, 276, https://doi.org/10.3390/atmos9070276.

——, C. D. Whiteman, S. W. Hoch, D. Jensen, E. R. Pardyjak, L. S. Leo, S. Di Sabatino, and H. J. S. Fernando, 2015: A case study of the nocturnal boundary layer evolution on a slope at the foot of a desert mountain. *J. Appl. Meteor. Climatol.*, **54**, 732–751, https://doi.org/10.1175/JAMC-D-14-0223.1.

——, M. W. Rotach, and F. Obleitner, 2019: A method to identify synoptically undisturbed, clear-sky conditions for valley-wind analysis. *Bound.-Layer Meteor.*, **173**, 435–450, https://doi.org/10.1007/s10546-019-00471-2.

Leukauf, D., A. Gohm, M. W. Rotach, and J. S. Wagner, 2015: The impact of the temperature inversion breakup on the exchange of heat and mass in an idealized valley: Sensitivity to the radiative forcing. *J. Appl. Meteor. Climatol.*, **54**, 2199–2216, https://doi.org/10.1175/JAMC-D-15-0091.1.

Mahrt, L., and S. Larsen, 1990: Relation of slope winds to the ambient flow over gentle terrain. *Bound.-Layer Meteor.*, **53**, 93–102, https://doi.org/10.1007/BF00122465.

Massey, J. D., W. J. Steenburgh, S. W. Hoch, and D. D. Jensen, 2017: Simulated and observed surface energy fluxes and resulting playa breezes during the MATERHORN field campaigns. *J. Appl. Meteor. Climatol.*, **56**, 915–935, https://doi.org/10.1175/JAMC-D-16-0161.1.

Matzinger, N., M. Andretta, E. V. Gorsel, R. Vogt, A. Ohmura, and M. W. Rotach, 2003: Surface radiation budget in an alpine valley. *Quart. J. Roy. Meteor. Soc.*, **129**, 877–895, https://doi.org/10.1256/qj.02.44.

McMillen, R. T., 1988: An eddy correlation technique with extended applicability to non-simple terrain. *Bound.-Layer Meteor.*, **43**, 231–245, https://doi.org/10.1007/BF00128405.

Nadeau, D. F., E. R. Pardyjak, C. W. Higgins, H. Huwald, and M. B. Parlange, 2013: Flow during the evening transition over steep alpine slopes. *Quart. J. Roy. Meteor. Soc.*, **139**, 607–624, https://doi.org/10.1002/qj.1985.

——, H. J. Oldroyd, E. R. Pardyjak, N. Sommer, S. W. Hoch, and M. B. Parlange, 2020: Field observations of the morning

transition over a steep slope in a narrow alpine valley. *Environ. Fluid Mech.*, **20**, 1199–1220, https://doi.org/10.1007/s10652-018-9582-z.

Papadopoulos, K. H., and C. G. Helmis, 1999: Evening and morning transition of katabatic flows. *Bound.-Layer Meteor.*, **92**, 195–227, https://doi.org/10.1023/A:1002070526425.

Rampanelli, G., D. Zardi, and R. Rotunno, 2004: Mechanisms of upvalley winds. *J. Atmos. Sci.*, **61**, 3097–3111, https://doi.org/10.1175/JAS-3354.1.

Rendón, A. M., J. F. Salazar, C. Palacio, and V. Wirth, 2015: Temperature inversion breakup with impacts on air quality in urban valleys influenced by topographic shading. *J. Appl. Meteor. Climatol.*, **54**, 302–321, https://doi.org/10.1175/JAMC-D-14-0111.1.

Reuten, C., D. G. Steyn, K. B. Strawbridge, and P. Bovis, 2005: Observations of the relation between upslope flows and the convective boundary layer in steep terrain. *Bound.-Layer Meteor.*, **116**, 37–61, https://doi.org/10.1007/s10546-004-7299-7.

Román-Cascón, C., and Coauthors, 2019: Comparing mountain breezes and their impacts on CO_2 mixing ratios in three contrasting areas. *Atmos. Res.*, **221**, 111–126, https://doi.org/10.1016/j.atmosres.2019.01.019.

Rotach, M. W., and Coauthors, 2022: A collaborative effort to better understand, measure and model atmospheric exchange processes over mountains. *Bull. Amer. Meteor. Soc.*, **103**, E1282–E1295, https://doi.org/10.1175/BAMS-D-21-0232.1.

Serafin, S., and D. Zardi, 2010: Structure of the atmospheric boundary layer in the vicinity of a developing upslope flow system: A numerical model study. *J. Atmos. Sci.*, **67**, 1171–1185, https://doi.org/10.1175/2009JAS3231.1.

——, and Coauthors, 2018: Exchange processes in the atmospheric boundary layer over mountainous terrain. *Atmosphere*, **9**, 102, https://doi.org/10.3390/atmos9030102.

——, and Coauthors, 2020: *Multi-Scale Transport and Exchange Processes in the Atmosphere over Mountains: Programme and Experiment*. Innsbruck University Press, 40 pp.

Triantafyllou, A. G., C. G. Helmis, D. N. Asimakopoulos, and A. T. Soilemes, 1995: Boundary layer evolution over a large and broad mountain basin. *Theor. Appl. Climatol.*, **52**, 19–25, https://doi.org/10.1007/BF00865504.

Vergeiner, I., and E. Dreiseitl, 1987: Valley winds and slope winds—Observations and elementary thoughts. *Meteor. Atmos. Phys.*, **36**, 264–286, https://doi.org/10.1007/BF01045154.

Wagner, J. S., A. Gohm, and M. W. Rotach, 2015: The impact of valley geometry on daytime thermally driven flows and vertical transport processes. *Quart. J. Roy. Meteor. Soc.*, **141**, 1780–1794, https://doi.org/10.1002/qj.2481.

Whiteman, C. D., 1982: Breakup of temperature inversions in deep mountain valleys: Part I observations. *J. Appl. Meteor.*, **21**, 270–289, https://doi.org/10.1175/1520-0450(1982)021<0270:BOTIID>2.0.CO;2.

——, 2000: *Mountain Meteorology: Fundamentals and Applications*. Oxford University Press, 355 pp.

——, and T. B. McKee, 1982: Breakup of temperature inversions in deep mountain valleys. Part II: Thermodynamic model. *J. Appl. Meteor.*, **21**, 290–302, https://doi.org/10.1175/1520-0450(1982)021<0290:BOTIID>2.0.CO;2.

——, and K. J. Allwine, 1985: VALMET—A valley air pollution model. Pacific Northwest Laboratory Final Rep. PNL-4728 Rev. 1, 176 pp., https://www.osti.gov/servlets/purl/5619570.

——, B. Pospichal, S. Eisenbach, P. Weihs, C. B. Clements, R. Steinacker, E. Mursch-Radlgruber, and M. Dorninger, 2004: Inversion breakup in small Rocky Mountain and Alpine

basins. *J. Appl. Meteor.*, **43**, 1069–1082, https://doi.org/10.1175/1520-0450(2004)043<1069:IBISRM>2.0.CO;2.

Wohlfahrt, G., A. Hammerle, G. Niedrist, K. Scholz, E. Tomelleri, and P. Zhao, 2016: On the energy balance closure and net radiation in complex terrain. *Agric. For. Meteor.*, **226–227**, 37–39, https://doi.org/10.1016/j.agrformet.2016.05.012.

Ye, Z. J., M. Segal, and R. A. Pielke, 1987: Effects of atmospheric thermal stability and slope steepness on the development of day-time thermally induced upslope flow. *J. Atmos. Sci.*, **44**, 3341–3354, https://doi.org/10.1175/1520-0469(1987)044<3341:EOATSA>2.0.CO;2.

Zardi, D., and C. D. Whiteman, 2013: Diurnal mountain wind systems. *Mountain Weather Research and Forecasting*, F. Chow, S. De Wekker, and B. Snyder, Eds., Springer Atmospheric Sciences, Springer, 35–119.

——, and S. Serafin, 2015: An analytic solution for time-periodic thermally driven slope flows. *Quart. J. Roy. Meteor. Soc.*, **141**, 1968–1974, https://doi.org/10.1002/qj.2485.

——, and Coauthors, 2021: The Bolzano Tracer Experiment (BTEX). *Bull. Amer. Meteor. Soc.*, **102**, E966–E989, https://doi.org/10.1175/BAMS-D-19-0024.1.

Zoumakis, N. M., and G. A. Efstathiou, 2006a: Parameterization of inversion breakup in idealized valleys. Part I: The adjustable model parameters. *J. Appl. Meteor. Climatol.*, **45**, 600–608, https://doi.org/10.1175/JAM2353.1.

——, and ——, 2006b: Parameterization of inversion breakup in idealized valleys. Part II: Thermodynamic model. *J. Appl. Meteor. Climatol.*, **45**, 609–623, https://doi.org/10.1175/JAM2354.1.